BULLETIN OF THE POLISH ACADEMY OF SCIENCES
TECHNICAL SCIENCES, Vol. 68, No. 3, 2020
DOI: 10.24425/bpasts.2020.133384

Research on ride comfort performance of a metal tire

Z. ZHENGLONG, S. BIN*, L. JIANGANG, D. ZHIGUANG, and H. ZHONGBO

Department of Vehicle and Electrical Engineering, Shi Jiazhuang Campus. AEU, Shi Jiazhuang 050003, China

Abstract. A new type of non-inflatable metal tire is designed to prevent the flat tire caused by puncture and shrapnel penetration, and it can be used on star rovers and military or civilian wheeled vehicles. In order to study vibration damping characteristics of the new wheel, a specimen with the same size as the pneumatic tire (235/70 R16) is made for contrast tests. A filtering method is proposed to reduce impulse and random interference noise in collected vibration signal. Comparative analysis of ride comfort performance is conducted by solving weighted acceleration root mean square (RMS) values. The results show that the filtering method has a good effect, and ride comfort of the metal tire is slightly worse, while it has a better grasping ability. Therefore, some extended structures have been recommended to improve the vibration damping performance.

Key words: metal tire, filtering method, ride comfort, extended structures.

1. Introduction

With the rapid development of automotive industry, vehicle's safety has been greatly improved, and more manufacturers focus on noise, vibration and harshness [1, 2]. The ride comfort refers to keeping the vibration and impact response of vehicles within a certain range to ensure the comfort of passengers and integrity of goods [3, 4]. At present, ride comfort testing is a common and reliable method to study vehicle vibration. In 1948, Janeway first proposed the method of human comfort, which reflects the sensitivity of human body according to the characteristics and values of vertical vibration. The correctness of this method was proved in 1960 [5]. In 1957, Dickman of Germany put forward K-factor method to analyze human comfort under sinusoidal signal vibration [6]. In 1968, Fred Pradko and Richard Lee conducted a series of unique vibration tests with precision instruments and test techniques. The response of human body to vibration in periodic and random environment can be judged in time domain and frequency domain by absorbing power method [7]. In 1974, ISO (International Organization for Standardization) issued ISO 2631-1974 to evaluate human health and comfort, human perception of vibration and motion diseases. Basic and auxiliary evaluation methods are specified when the peak coefficient of vibration waveform is greater than or less than 9 [8]. In 1987, the British Standard BS 6841-1987 on ride comfort was issued. The vibration dose value evaluation method including the indicator RMS and RMQ was used to evaluate [9]. In the test process, there is lots of strong random and impulse noise in collected vibration signal, because of the influence of frame vibration, environmental and electrical noise. As a result, the solutions of RMS values can be directly affected [10]. Therefore, it is necessary to eliminate interference of obvious noise and retain effective amplitude information of the signal before performing ride comfort analysis.

Wavelet transform method is sensitive to signal mutations, which has high time resolution at high frequency, high frequency resolution at low frequency. In Ref. [11], the difference of transfer characteristics for signal and noise in multi-scale space is used to conduct effective detection under interference. While filtering method based on wavelet transform lacks adaptability. Empirical mode decomposition (EMD) method breaks through "prior" defect of signal processing and relies on signal itself for adaptive decomposition. On the basis of Ref. [12], Flandrin [13] proposed the idea of filter bank based on EMD, i.e., an adaptive combination of high-pass, low-pass, band-pass or band-stop filters by selecting corresponding intrinsic mode function (IMF). So far, many algorithms for different applications based on EMD have been proposed [14–16].

In the article, an innovative structure of non-pneumatic metal tire is designed. Test system for tire ride comfort is built based on a 6×6 unmanned vehicle. Vibration signal on different positions and at different speeds are measured. Aiming at the problem of interference noise mixed in collected vibration signal, a method combing the morphological and EMD methods is proposed. The signal filtering process is as follows: Firstly, the instantaneous pulse and strong random noise are filtered by morphological filter method, and the signal details are kept as much as possible. Then the signal is decomposed into many IMFs by EMD, noise IMFs are screened and eliminated according to similarity theory. Finally, the residual effective modal components are reconstructed.

2. Filtering methods for vibration signal

2.1. Morphological method. Morphological filter method is nonlinear based on mathematical morphology. Its idea is to de-

*e-mail: 7583288long@163.com

Manuscript submitted 2019-12-02, revised 2020-01-07, initially accepted for publication 2020-01-18, published in June 2020

sign a probe called structural element to match and modify the signal, so as to effectively extract the edge contour and maintain main morphological characteristics. There are four basic operations: corrosion, expansion, morphological open operation and morphological close operation [17]. Suppose $f(n)$ and $g(n)$ be the functions defined in two discrete domains $F = \{0,1,\ldots,N-1\}$ and $G = \{0,1,\ldots,M-1\}$. If $N > m$, $f(n)$ is the input signal, and $g(n)$ is the structural element. The corrosion and expansion operations of $f(n)$ on $g(n)$ are given by:

$$(f \ominus g)(n) = \min_{m=1,2,\ldots,M} \{f(n+m) - g(m)\}, \tag{1}$$

$$(f \oplus g)(n) = \max_{m=1,2,\ldots,M} \{f(n-m) + g(m)\}. \tag{2}$$

The morphological open and close operations are given by:

$$(f \circ g)(n) = (f \ominus g \oplus g)(n), \tag{3}$$

$$(f \bullet g)(n) = (f \oplus g \ominus g)(n). \tag{4}$$

In order to suppress both peak and low noise, morphological open-close and close-open filters are constructed, and given by:

$$OC(f(n)) = (f \circ g \bullet g)(n), \tag{5}$$

$$CO(f(n)) = (f \bullet g \circ g)(n). \tag{6}$$

Due to the anti-expansibility of morphological open operation and expansibility of morphological close operation, there is a statistical deflection in the process of morphological filtering. Therefore, a combination filter of open-close and close-open can be constructed by cascading open and close operations, which is given by:

$$y(n) = [OC(f(n)) + CO(f(n))]/2. \tag{7}$$

Structural element types of linear, triangular, semicircle, sinusoidal are commonly used. Engineering application experience shows that there is a good filtering effect on random noise for semi-circular structural element, and on impulse noise for triangular structural element [18]. In addition, long structural element reaches good noise reduction while blurs the details of the signal. Short structural element keeps the signal details better while is not good for noise reduction. Therefore, the proper morphological filter should be selected according to actual requirements.

2.2. The EMD method

2.2.1. Decomposition principle of EMD. Different from the method of Fourier and wavelet decomposition, EMD method adaptively generates several IMFs according to time-scale characteristics of signal [19, 20]. EMD decomposition process can be described as

Step 1. Determine all maximum and minimum points of the signal $s(t)$ to be processed.

Step 2. Connect the maximum point and minimum point to form upper and lower envelope curve. $h1(t)$ is the difference that signal $s(t)$ minus the mean of upper and lower envelope.

Step 3. Judge whether $h_1(t)$ meets the constraint conditions of IMF. If not, repeat steps 1 and 2 with $h_1(t)$ as new $s(t)$ until $h_{1k}(t)$ meets the IMF conditions, and $h_{1k}(t)$ as the IMF component c_1 of $s(t)$.

Step 4. c_1 is separated from $s(t)$, and the remaining signals repeat above filtering steps until the signal can't be decomposed, and the trend term rn of the signal is obtained. Then intrinsic modal components and trend terms are used to express original signal, which is given by:

$$s(t) = \sum_{k=1}^{n} c_k(t) + r_n(t). \tag{8}$$

2.2.2. The EMD noise reduction method. Decomposed IMFs are arranged in order of frequency from high to low [21]. They are screened by solving correlation coefficients between each component and original signal [22, 23]. According to similarity theory, the meanings of correlation coefficient values are shown in Table 1.

Table 1
Relationship between correlation coefficient and correlation degree

Correlation coefficient	Correlation degree
$0.00-\pm0.30$	Micro related
$\pm0.30-\pm0.50$	Real related
$\pm0.50-\pm0.80$	Significant related
$\pm0.80-\pm1.00$	High related

2.3. Comparative analysis of different filtering methods. In order to compare the filtering effect of several commonly used filtering methods, the signal curves processed by the method of low-pass filtering, wavelet threshold and morphology-EMD filtering are presented, as shown in Fig. 1. Low-pass filtering can remove high-frequency noise interference, but there is still some low-frequency noise, and the peak values of useful signal are weakened. Wavelet threshold method can effectively eliminate random noise of the signal, but it gets little suppression effect on strong impulse noise. And the morphology-EMD filtering method can well retain waveform of useful signal while eliminating obvious random and impulse noise.

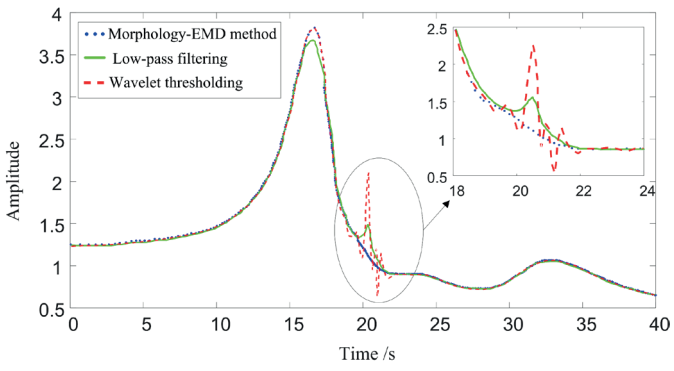

Fig. 1. Filtering results under different de-nosing methods

To evaluate the processing effects of above methods quantitatively, signal-to-noise ratio (SNR) and root mean squared error (RMSE) are calculated according to equations (9) and (10). SNR represents the ratio between signal and noise. The larger the SNR value is, the smaller the noise mixed in signal is, which indicates there is a high-quality signal. RMSE is used to evaluate the distortion rate of waveform. And the smaller the RMSE value is, the better the effect of noise reduction is:

$$\mathrm{SNR} = 10\lg\left\{\frac{\sum_{n=1}^{N} s^2(n)}{\sum_{n=1}^{N}\left[s(n)-\hat{s}(n)\right]^2}\right\}, \tag{9}$$

$$\mathrm{RMSE} = \sqrt{\frac{1}{N}\sum_{n=1}^{N}\left[s(n)-\hat{s}(n)\right]^2}, \tag{10}$$

where $s(n)$ is the original signal, $\hat{s}(n)$ is the estimated signal after noise reduction, N is the number of sampling points. Calculation results of SNR and RMSE are shown in Table 2. As can be seen from the table, the method proposed in this paper has a better filtering effect.

Table 2
SNR and RMSE of different noise reduction algorithms

De-noise methods	SNR/dB	RMSE/Gs
low-pass filtering	43.909	0.142
wavelet threshold	48.607	0.130
method in this paper	51.013	0.115

3. Structure design of the metal wheel

On the basis of previous research results of the research group [24, 25], structural improvement and optimization have been carried out, and the new metal tire composition is shown in Fig. 2. The tire body is mainly composed of main spring (blue), auxiliary spring mesh (gray), fixed belt (bright yellow), side chucks (dark yellow) and rim (black) with helical groove. The main spring is formed by a thick helical spring which is connected end to end to form an internal support body. Several auxiliary springs with the same rotation direction and pitch hook up with each other to form the auxiliary spring mesh. Some auxiliary springs go through the main spring wire to ensure the structural integrity of the main and auxiliary springs. The main spring is stuck into the helical groove on the rim surface and tightened by fixed belts and fastening bolts. Bolts are used to fix the auxiliary spring mesh on both sides of the rim and the position is limited through the U-shaped holes on the chucks. The main spring bears most loads and torques, the auxiliary spring mesh bears some loads and enhances the stability and ground adhesion of the tire.

4. Ride comfort analysis of the metal wheel

4.1. Vertical vibration analysis. A three-axle 6×6 vehicle in laboratory has a simple chassis without suspension system, speed reducer etc., as shown in Fig. 3(a). Therefore, the vibration caused by road roughness directly acts on vehicle body after passing through the wheels. A simplified half vehicle vibration model is established, as shown in Fig. 3(b). In Fig. 3(b), k_t and c_t are stiffness and damping of the wheel respectively, q_f, q_m and q_r are road excitation of front, middle and rear wheels respectively, and m is the vehicle mass.

Tire is the only component used to reduce vibration during driving process for above vehicle. Whole vehicle body including the frame and radar, etc. is regarded as on-wheel mass. Thus, a single mass model for analyzing the vehicle vertical vibration is established, as shown in Fig. 3(c). In Fig. 3(c), m, k and c are on-wheel mass, wheel equivalent stiffness and wheel equivalent viscous damping ratio, respectively, and q is the road roughness function.

Without considering damping influence, resonant frequency of on-wheel mass is approximately calculated by:

$$f \approx \frac{1}{2\pi}\sqrt{\frac{k}{m_2}}. \tag{11}$$

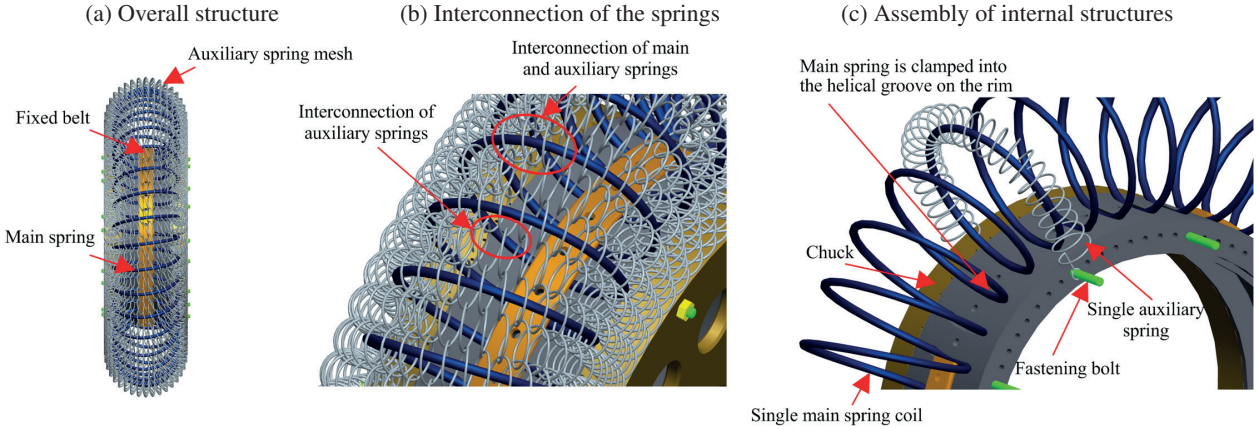

Fig. 2. Structural diagram of the metal tire

(a) Three-axle 6 × 6 vehicle (b) Half vehicle vibration model (c) Single mass analysis model

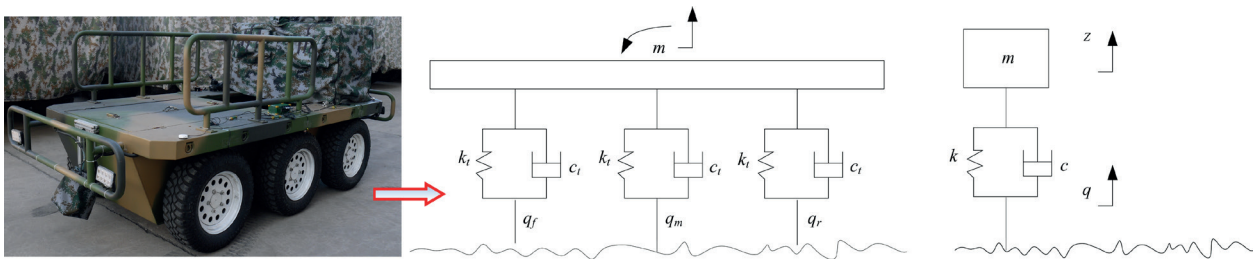

Fig. 3. Analysis of vehicle vertical vibration

In order to weaken vehicle vibration, the resonant frequency must be reduced effectively. According to equation (11), smaller resonance frequency can be obtained by reducing the wheel stiffness or increasing the on-wheel mass.

4.2. Ride comfort tests. Ride comfort tests of metal and pneumatic wheels are carried out based on a 6 × 6 vehicle, as shown in Fig. 4(a). Test system is shown in Fig. 4(b). And the installation positions of acceleration sensors are marked in the figure. Sensors are fixed on inside of the vehicle body and right above the wheel axles. The bottom of the sensor is equipped with a matching magnet base, which can be adsorbed on the vehicle body. And the positions can better reflect the vibration degree of wheel. Vehicle runs on a flat cement road and a square tube with section size of 50 × 25 mm is set for impact vibration test, as shown in Fig. 4(c).

(a) 6 × 6 unmanned vehicle

(b) Test system (c) Set a square tube

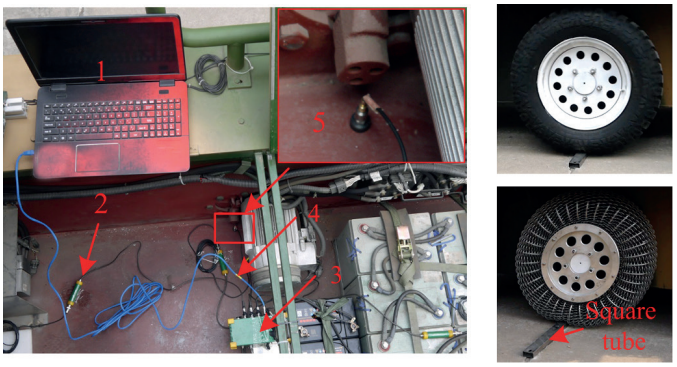

Fig. 4. Ride comfort test system

Equipment of the test system in Fig. 4(b) is shown in Fig. 5 below.

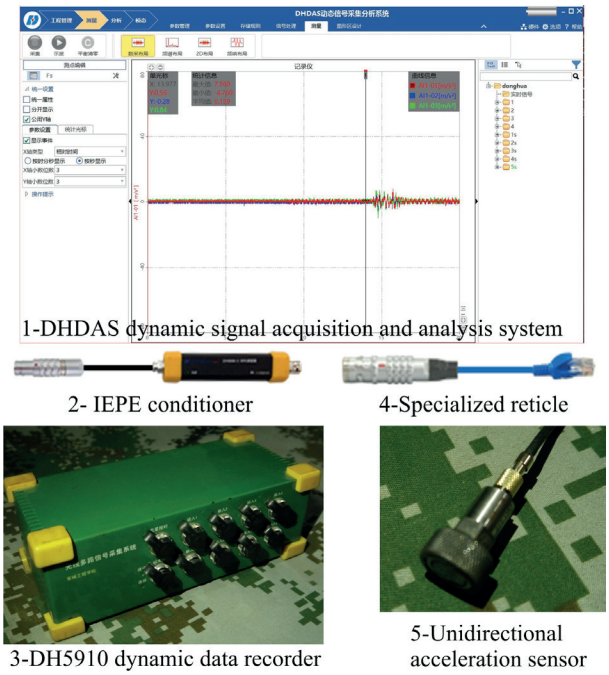

Fig. 5. Equipment of test system

IEPE piezoelectric acceleration sensors are used, and its parameters are shown in Table 3.

Table 3
Parameters of DH131E piezoelectric acceleration sensor (IEPE)

Characteristic	Parameter	Characteristic	Parameter
Type and characteristics	Generally for vibration and shock	Lateral sensitivity ratio	$< 5\%$
Sensitivity ($mV/m \cdot s^{-2}$)	1	Output lead position	Top
Install resonance frequency (Hz)	44	Internal structure form	Shear
Frequency range (Hz)	1∼10000	Use temperature (°C)	−20∼120
Maximum measured acceleration ($m \cdot s^2$)	5000	Mass (g)	5.5
Use limit ($m \cdot s^2$)	10000	Outline size (mm)	$\phi 10 \times 16$

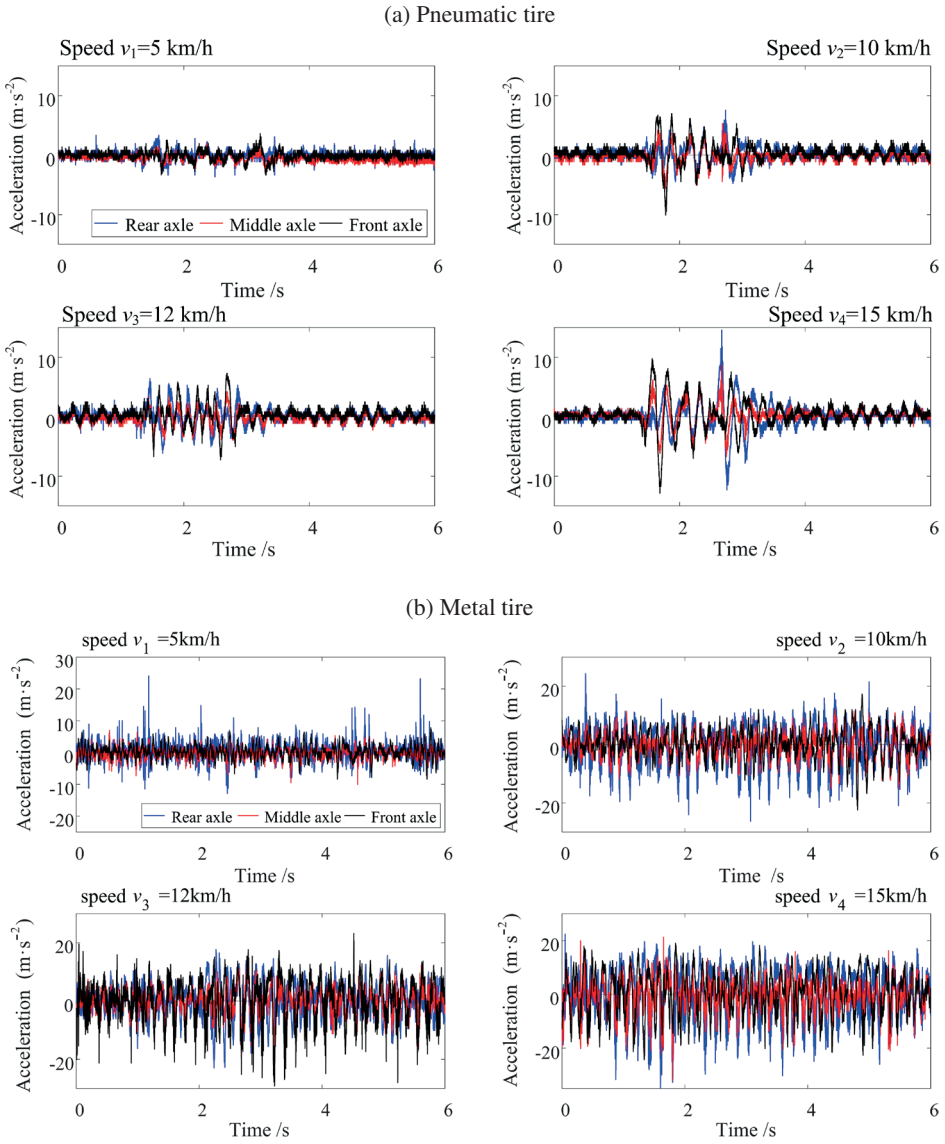

Fig. 6. Time domain curves of the vibration signal

Signal collected by acceleration sensors are modulated and amplified by conditioner and then transmitted to data recorder. Laptop stores the data in real time via a network cable. Time-domain curves are shown in Fig. 6. And the measured vibration signal contains a large number of impulse and random noise obviously, which will have a great impact on the ride comfort analysis results.

4.3. Vibration signal filtering. The processing flow of vibration signal filtering and vehicle ride comfort analysis process is shown in Fig. 7.

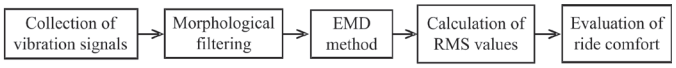

Fig. 7. Flow chart of vibration signal processing

Acceleration data of each wheel under 12 working conditions (at 4 different speeds and on different 3 positions) needs to be processed. As an example to show the filtering process, vibration signal at speed of 5 km/h and on rear axle position is selected. And the signal processing under other working conditions is the same. According to the characteristics of noise in vibration signal, triangular structural elements whose length is slightly longer than the duration of impulse noise are selected to form a combined morphological filter according to equation (7). The vibration signal before and after filtering is shown in Fig. 8.

After that, the signal in Fig. 8 is decomposed by EMD, and the results are shown in Fig. 9.

According to the figures above, vibration signal of pneumatic and metal tire are divided into 10 and 11 IMFs respectively. Each group also includes a trend term *res*. Tables 4 and 5 respectively show interrelation coefficients solutions of each IMF for pneumatic and metal tires.

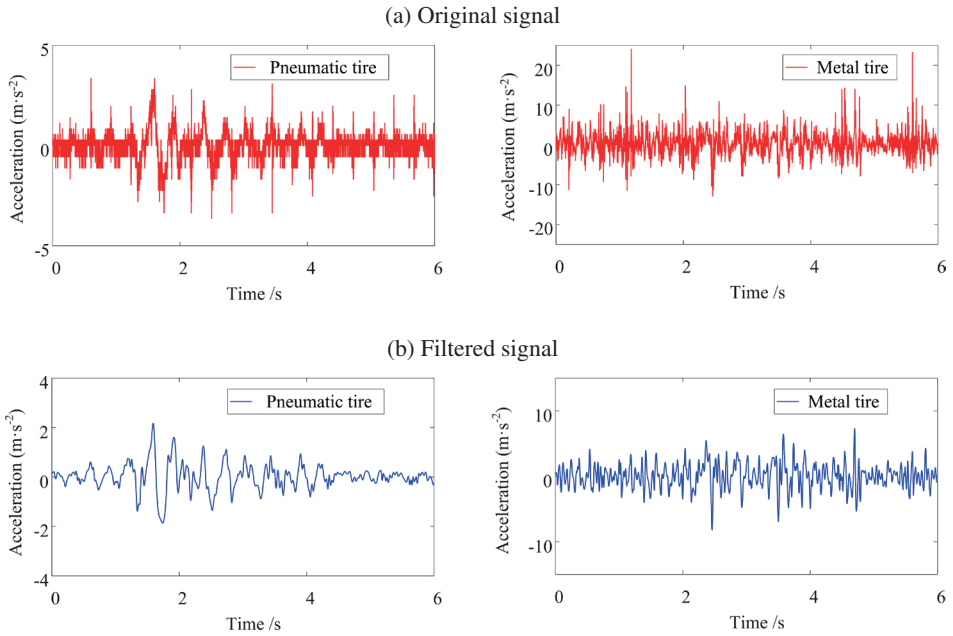

Fig. 8. Time domain curves of the vibration signal

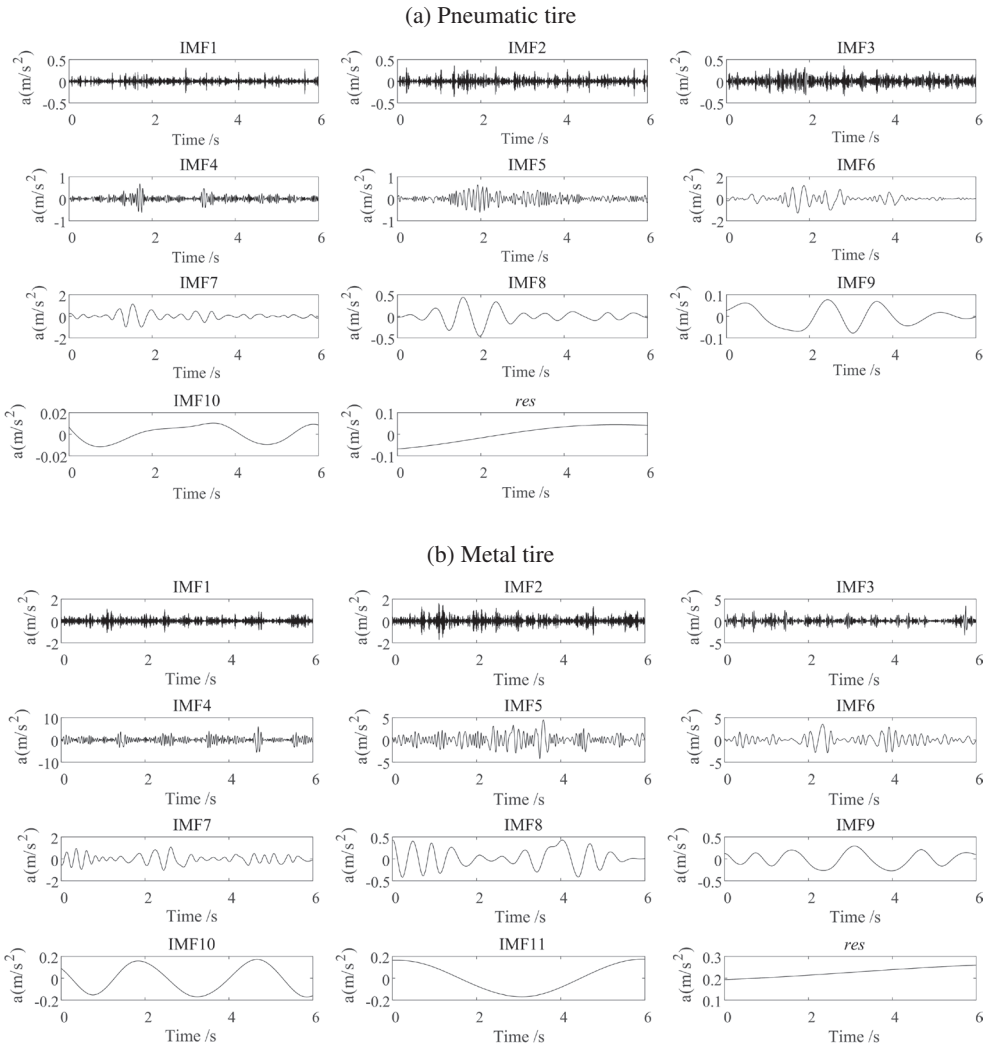

Fig. 9. EMD decomposition results

Table 4
Interrelation coefficients of the pneumatic tire

Component	Cross-correlation coefficient	Component	Cross-correlation coefficient	Component	Cross-correlation coefficient
IMF1	0.0159	IMF5	0.3131	IMF9	0.0106
IMF2	0.1188	IMF6	0.6686	IMF10	0.0090
IMF3	0.1491	IMF7	0.6478		
IMF4	0.2034	IMF8	0.1965		

Table 5
Interrelation coefficients of the spring tire

Component	Cross-correlation coefficient	Component	Cross-correlation coefficient	Component	Cross-correlation coefficient
IMF1	−0.0053	IMF5	0.5423	IMF9	−0.0014
IMF2	0.1006	IMF6	0.4330	IMF10	0.0097
IMF3	0.2921	IMF7	0.1637	IMF11	−0.0037
IMF4	0.5414	IMF8	0.0437		

According to Table 1, the real correlation (correlation coefficient is greater than 0.3) IMFs should be selected, i.e., IMFs 5∼7 of pneumatic tire and IMFs 4∼6 of metal tire are for composition and reconstruction. The same way is used to preprocess the vibration signal under other working conditions, and the time-domain acceleration signal are obtained, as shown in Fig. 10.

It can be seen from above figures that the front axle of pneumatic tire (black line) has largest vibration amplitudes, followed by the rear axle (blue line). There is a maximum value of vi-

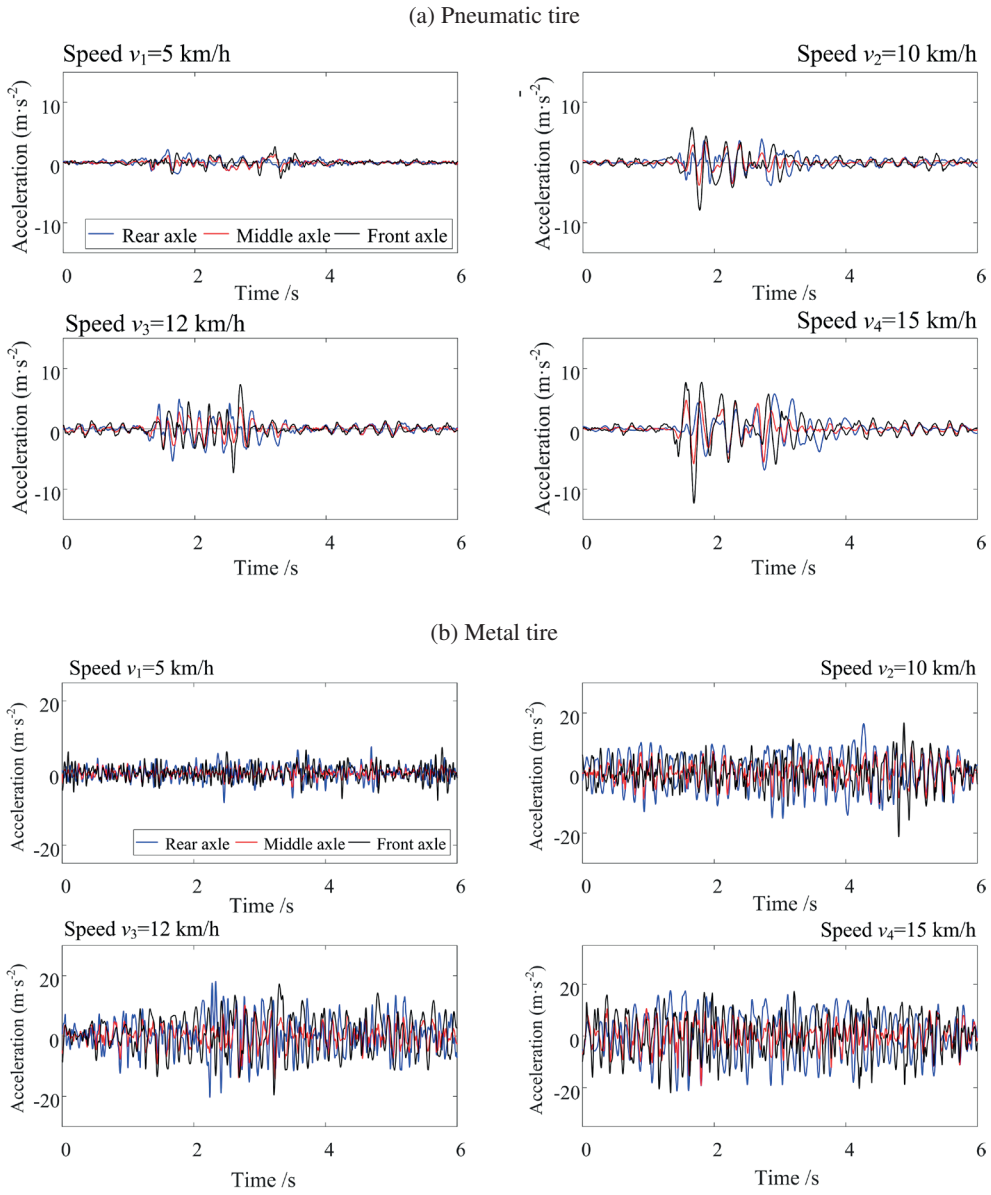

Fig. 10. EMD decomposition results

bration amplitude on rear axle of metal tire, followed by front axle. And amplitude at middle axle for both tires is the smallest. While test results should be quantitatively processed according to vehicle ride comfort theory for accurate analysis.

4.4. Ride comfort evaluation. At present, there are subjective and objective evaluation methods on evaluating vehicle ride comfort. Subjective method relies on intuitive feelings of experienced testers, which is direct but fuzzy. Objective method is evaluated according to actual measured data, which has been used widely because of its accuracy excluding individual subjective difference.

Most common test standard in the world is ISO 2631-1997 [26]. Similar standards have also been set up in many countries, such as VDI 2057-2002 in Germany [27], GB/T 4970-2009 in China [28] and SAE J 1940-2011 in the U. S [29]. When peak coefficient of vibration waveform is less than 9, RMS can be used to evaluate the influence of vibration on human comfort. Peak coefficient represents the ratio of the peak value of the weighted acceleration time history aw(t) to the weighted acceleration root mean square value a_w. Applicable frequency range is 0.5∼80 Hz.

Calculation of RMS is given by:

$$a_w = \left[\int_{0.5}^{80} W^2(f) G_a(f) \, \mathrm{d}f \right]^{1/2}, \tag{12}$$

where $G_a(f)$ is the power spectral density function obtained through spectrum analysis of the collected acceleration-time course $a(t)$, and $W(f)$ is the frequency weighting function.

According to relevant definitions for vertical axial line vibration of the seat support surface in the standard, the expression of the frequency weighting function $W(f)$ (asymptote) is given by:

$$W_k(f) = \begin{cases} 0.5 & (0.5 < f < 2) \\ f/4 & (2 < f < 4) \\ 1 & (4 < f < 12.5) \\ 12.5/f & (12.5 < f < 80) \end{cases} \tag{13}$$

where the unit of frequency f is Hz.

By solving power spectral density and substituting them into equation (12), RMS values of pneumatic and metal tires under various working conditions are obtained, as shown in Tables 6 and 7.

As can be seen from above tables, ride comfort of the two kinds of tires at all positions becomes worse with the increase of speed. And the influence of different speeds on metal tire is greater than that on pneumatic tire. In the acceleration process from 15 km/h to 25 km/h, RMS of the pneumatic tire becomes 3∼3.4 times of the original, the one of metal tire is 3.4∼3.6 times. And the position of the rear side of the vehicle is more sensitive to changes in speed than the front.

In terms of vibration on different positions, the best ride comfort is in the middle of vehicle body for two kinds of tires. The

Table 6
RMS values of the pneumatic tire (m/s^2)

Position	Speed (km/h)			
	15	25	30	35
Rear axle	0.36	0.85	1.00	1.24
Middle axle	0.34	0.65	0.83	1.05
Front axle	0.49	0.99	1.19	1.48

Table 7
RMS values of the metal tire (m/s^2)

Position	Speed (km/h)			
	15	25	30	35
Rear axle	1.86	5.06	5.79	6.78
Middle axle	1.11	2.76	3.60	3.72
Front axle	1.77	3.73	5.40	6.04

performance of rear wheel is better than that of front wheel for pneumatic tire, while it is the opposite for metal tire. According to the actual observation in the test (Fig. 4), when the front wheel passes through the square tube for the first time, the vehicle body will jump up to a certain height. Large elasticity of the pneumatic tire makes the front wheel vibrate frequently. As the radar and other guiding equipment are installed in the front and the battery pack is arranged in the back, the overall gravity center is located at the rear. The gravity position further increases the vibration degree of the front wheel when the vehicle passes obstacles.

When metal tire passes through the square tube, the mesh surface can produce a large deformation to completely cover the tube, which makes grasping stronger. And because the sprung mass of rear wheel is larger, the vibration caused by gravity is more difficult to be eliminated when the rear wheel passes obstacles which make the rear wheel have a worse ride comfort.

For both tires, when vehicle is driving on a flat road, tires will not be excited by the ground pulse. Up-down oscillation caused by gravity will have less effect on body vibration, and the closer the position is to gravity center, the smaller the vibration should be. Therefore, vibration on flat road is further tested. Original and preprocessed signal is shown in Figs. 11 and 12.

Solved RMS values on flat road are shown in Tables 8 and 9.

Table 8
RMS values of the pneumatic tire on flat road (m/s^2)

Position	Speed (km/h)			
	5	10	12	15
Rear axle	0.06	0.07	0.12	0.15
Middle axle	0.05	0.08	0.09	0.11
Front axle	0.09	0.09	0.15	0.16

(a) Pneumatic tire

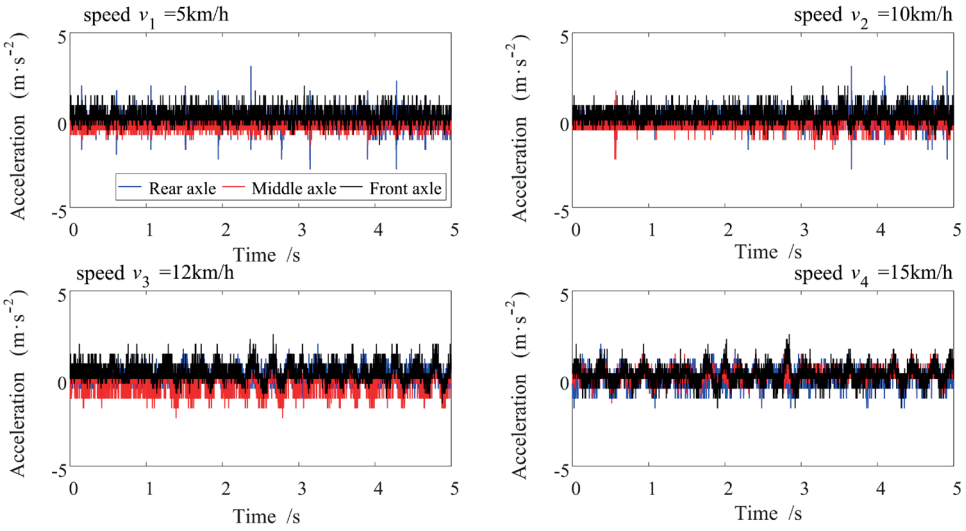

(b) Metal tire

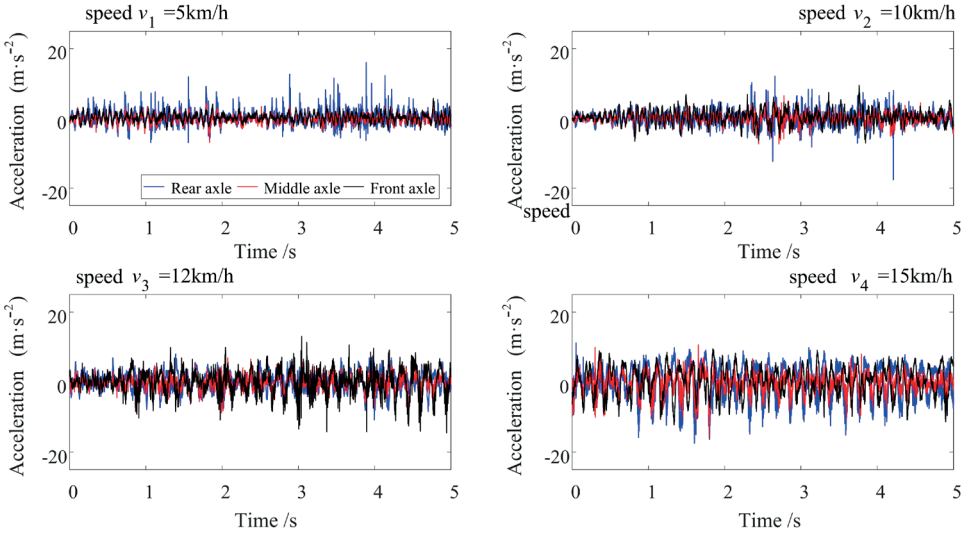

Fig. 11. Original vibration signal on flat road

(a) Pneumatic tire

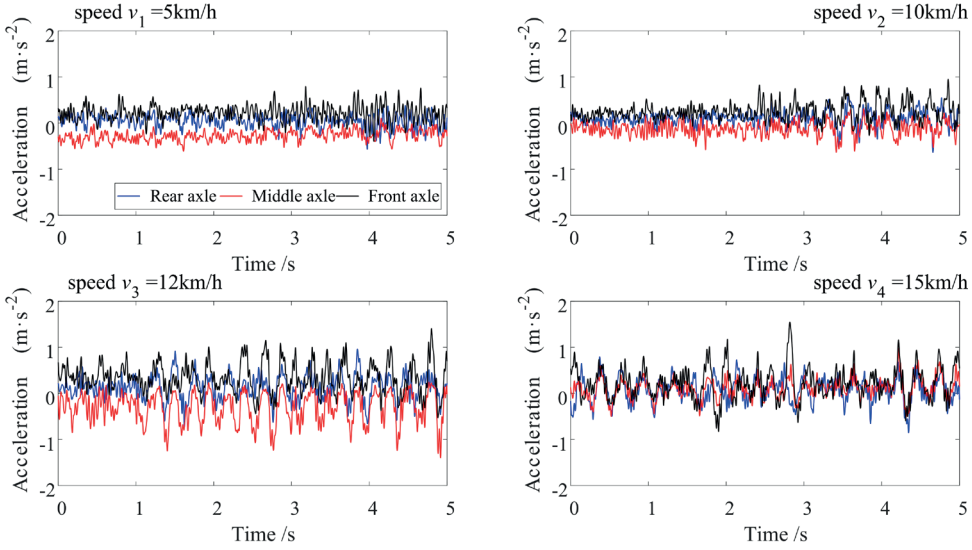

(b) Metal tire

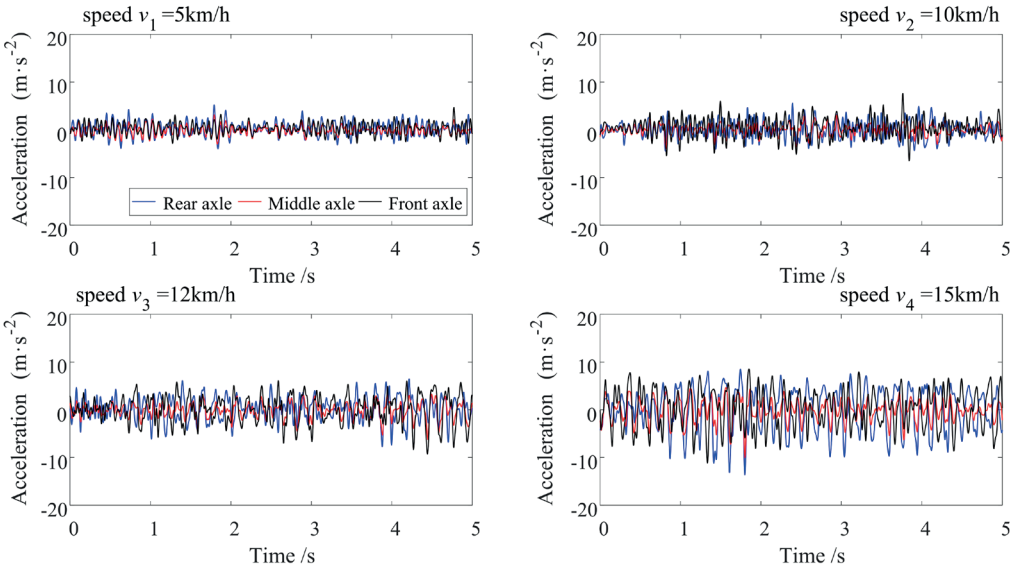

Fig. 12. Preprocessed vibration signal on flat road

Table 9
RMS values of the metal tire on flat road (m/s^2)

Position	Speed (km/h)			
	5	10	12	15
Rear axle	0.71	1.18	1.43	2.26
Middle axle	0.60	0.75	0.92	1.43
Front axle	0.91	1.34	1.55	2.53

It can be seen from above tables that the ride comfort of the rear wheel is better than that of the front for both tires on flat road. The reason is that the vehicle gravity center is located in rear position. When the wheels roll slowly at a uniform speed on flat road, the farther away from the gravity center, the more difficult it is to eliminate the vibration caused by road roughness. The results are consistent with the previous analysis.

5. Extended structures of the metal tire

There are two ways to solve the problem of the metal tire having a worse ride comfort. One is to change structural parameters, such as, reducing spring diameter or changing material for smaller spring mesh stiffness. The other is to optimize the tire structure.

All-metal structure designed in Fig. 2 can be used in the vacuum and high temperature environment where the rubber tire cannot be used. Fig. 13(a) shows a pneumatic/non-pneumatic structure. The inner air-tight layer is used to seal gas from leakage for good elasticity and vibration absorption. When gas leaks away, the metal spring mesh starts to support and maintain normal vehicle running. Fig. 13(b) shows a metal wheel filled with foam balls. Foam balls are mainly made of artificial or discarded material, which has the characteristics of low apparent density and high strength. Fig. 13(c) shows a wheel-tracked moving structure with a strong gripping, climbing and cross-country ability.

Above extended structures are based on the metal tire discussed in this paper, and the metal spring mesh plays a ma-

(a) A pneumatic/non-pneumatic safety tire

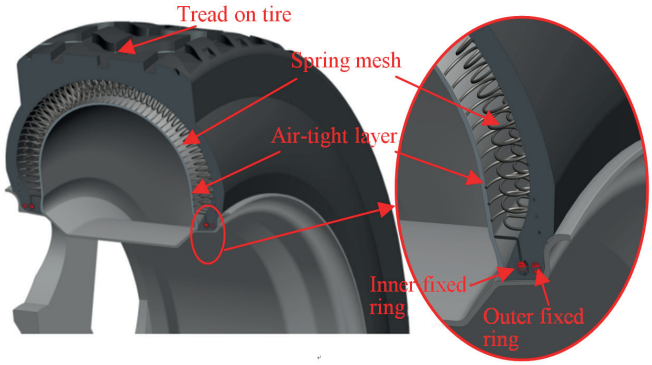

(b) A metal spring mesh wheel filled with foam balls

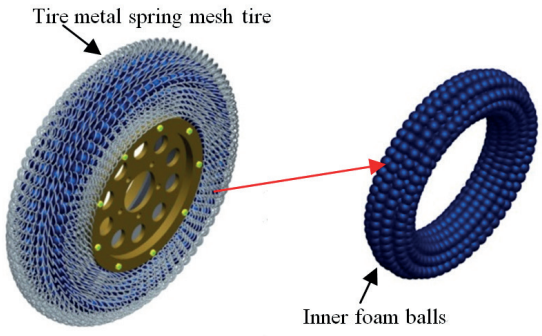

(c) A wheel-tracked moving structure

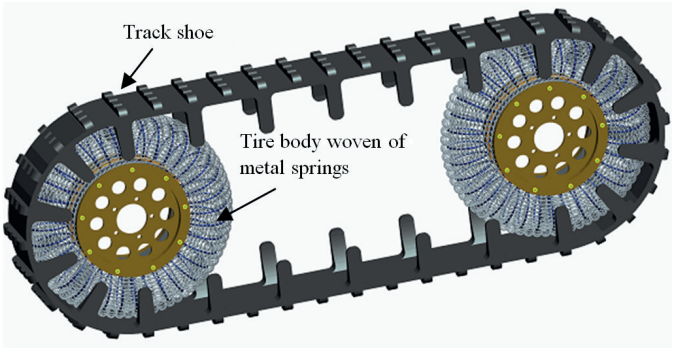

Fig. 13. Extended structures of the metal tire

jor supporting structure. Each tire structure not only keeps the similar load-bearing, damping and traction characteristics with the pneumatic rubber tire, but also has the advantages of penetration resistance, non-inflation, wide usage temperature range, green environmental protection, etc. Therefore, the extended structures have a certain positive role and guiding significance for further improvement of the current metal tire.

6. Conclusions

Comparative analysis of different filtering methods, ride comfort test, vibration signal preprocessing and evaluation on the vehicle equipped with pneumatic and metal tires are carried out in the paper. The following conclusions are obtained:

(1) A filtering method combined with morphological and EMD method is proposed. Impulse and environmental noise in vibration signal can be well removed through the method. And the signal can be decomposed into multiple IMFs according to the frequency, which provides a means for tire vibration spectrum analysis in future studies.

(2) The test results show that the ride comfort performance of metal tire is little worse than that of pneumatic tire. But when the tire passes through obstacles such as a square tube, the spring mesh surface of metal tire will produce greater stress deformation, so as to wrap the obstacles inside, making the tire produce small vibration. Therefore, the metal tire has a better grasping performance.

(3) Vertical vibration is mainly affected by the mass and vertical stiffness of the tire. In order to improve the ride comfort performance, pitch diameter and wire diameter of the main and auxiliary springs need to be modified or the wheel surface has to be covered with rubber. And extended metal tire structures have been proposed, which need to be further studied by the way of structure optimization, specimen processing and testing.

Acknowledgements. This work was supported by the (China) National Science and Technology Project Fund under grant No. A07 2004044. And the authors appreciate the reviewers and editors for their useful criticisms and comments.

References

[1] H. Cho, S. Kim, and M. Kim, "Multiple quantile regression analysis of longitudinal data: Heteroscedasticity and efficient estimation", *J. Multivar. Anal.* 155, 334–343 (2017).

[2] J. Andert, K. Herold, R. Savelsberg, and M. Pischinger, "NVH optimization of range extender engines by electric torque profile shaping", *IEEE Trans. ControlSyst. Technol* 25 (4), 1465–1472 (2017).

[3] G.R. Muller, Ch. Neuper, and G. Pfurtscheller, "Numerical study of selected military vehicle chassis subjected to blast loading in terms of tire strength improving", *Bull. Pol. Ac.: Tech.* 63 (4), 867–878 (2015).

[4] P. Baranowski and J. Malachowski, "Numerical study of selected military vehicle chassis subjected to blast loading in terms of tire strength improving", *Bull. Pol. Ac.: Tech.* 63 (4), 867–878 (2015).

[5] R.N. Janeway, "Human Vibration Tolerance Criteria and Applications to Ride Evaluation", Instrumentation, 1975.

[6] D.D. Sheng, "Research on Virtual Roadway Test System and Evaluation Method for Vehicle Ride Comfort based on New Test Regulation", *Anhui Agricultural University*, An Hui 2013.

[7] R. Lee and F. Pradko, "Analytical Analysis of Human Vibration", SAE Technical Paper 680091, Human Factors, 1968.

[8] S.A. Chen, R. He, and S.L. Lu, "Evaluating system of vehicle ride comfort", - *Journal of Jiangsu University (Natural Science Edition)* 27 (3), 229–233 (2006).

[9] BS6841-1987, "Measurement and Evaluation of Human Exposure to Whole-body Mechanical Vibration and Repeated Shock", BSI, 1987.

[10] J. Wang, *Application of MATLAB in Vibration Signal Processing*, Beijing: China Water&Power Press, Bei Jing 2006.

[11] D.L. Donoho, "De-noising via soft-thresholding IEEE Trans", *On Inform. Theory* 41 (3), 613–627 (1995).

[12] Z.H. Wu and N.E. Huang, "A study of the characteristics of white noise using the empirical mode decomposition method", *Proc. Roy. Soc. London* A460, 1597–1611 (2004).

[13] P. Flandrin, "Empirical mode decomposition as a filter bank", *IEEE Signal Processing Letters* 11 (2), 112–114 (2003).

[14] J.A. Nimunkar and J.W. Tompkins, "EMD-based 60-Hz noise filtering of the ECG", *Proceedings of the 29th Annual Intemational Conference of the IEEE EMBS Cite Intemationale* 8, pp. 1904–1908 (2007).

[15] V. Agarmal, and H.L. Tsoukalas, "Denoising electrical signal via Empirical Mode Decomposition", *2007 Ireq Symposium-Bulk Power System Dynamics and Control-VIII, Revitalizing Operational Reliability*, pp. 1519–1525 (2007).

[16] P. Flandrin, P. Goncalves, and G. Rilling, "Detrending and denoising with empirical mode decomposition", *In Proceeding of XII EUSIP CO2004, Austria*, pp. 1022–1029P (2004).

[17] C.H. Zhao, and S.H. Sun, "Adaptive complex ranked-ordermorphological filtering", *Systems Engineering and Electronics* 20 (7), 57–60 (1997).

[18] Z.C. Lu, D. Mi, Z.S. Xu, et al., "Research in application of multiscale and multi-element morphlogical filtering in geomagnetic orientation", *Journal of Hebei University of Science and Technology* 32 (3), 228–232 (2011).

[19] S. Jiao, W. Li, and M. Yang, "Validation of simulation models based on empirical modal decomposition and grey relevance analysis", *J. Syst. Eng. Electron.* 35 (12), 2643 (2013).

[20] J. Li, "Study on the characteristics and compensation method of vehi-cleinterferential magnetic fielding eomagnetic measurment", National University of Defense Technology, Chang Sha 2013.

[21] W.D. Jiao, Y.H. Jiang, and S.S. Pu, "Modified Signal de-noising approach for multiplicative noise based on empirical mode decomposition", *J. Mech. Eng*. 51 (24), 1–8 (2015).

[22] J. Dang, "Research on methods of vibration signal processing and incipient fault identification for large rotating machine", Xi'an: Xi'an University of Technology, Xi'an, 2018.

[23] Y. Huang, "Research on fault diagnosis of bearing based on vibration signal denoise and decomposition", Xi'an: Xi'an University of Technology, Xi'an, 2018.

[24] S. Bin, Z. Zhongzhi, L. Jiangang, et al., "Finite Elements Analysis of a Spring Tire", *Mechanical Science and Technology for Aerospace Engineering* 35 (02), 303–308 (2015).

[25] Z.-Z. Zhang, J.-G. Lü, B. Song, and F. Gao, "Structural design and analysis of a new type of spring tire", *J. Vib. Shock* 32 (21), 119–124 (2013).

[26] ISO 2631-1-1997- "Mechanical vibration and shock-evaluation of human exposure to whole-body-vibration. Part 1: General requirements", International Standard Organization, 1997.

[27] VDI 2057-2002, "Human exposure to mechanical vibration whole-body vibration", Verein Deutcher Ingenieure (VDI), 2002.

[28] GB/T 4970-2009, "Method of running test – Automotive ride comfort", Beijing: Standards Press of China, 2009.

[29] SAE J 1490, "Measurement and presentation of truck ride vibrations", Society of Automobile Engineers, 2011.